Behavioral/Cognitive

Neuroimaging Signatures of Metacognitive Improvement in Sensorimotor Timing

Farah Bader and Martin Wiener
Department of Psychology, George Mason University, Fairfax, Virginia, 22030

Error monitoring is an essential human ability underlying learning and metacognition. In the time domain, humans possess a remarkable ability to learn and adapt to temporal intervals, yet the neural mechanisms underlying this are not clear. Recently, we demonstrated that humans improve sensorimotor time estimates when given the chance to incorporate previous trial feedback (Bader and Wiener, 2021), suggesting that humans are metacognitively aware of their own timing errors. To test the neural basis of this metacognitive ability, human participants of both sexes underwent fMRI while they performed a visual temporal reproduction task with randomized supra-second intervals (1.5–6 s). Crucially, each trial was repeated following feedback, allowing a "re-do" to learn from the successes or errors in the initial trial. Behaviorally, we replicated our previous finding of improved re-do trial performance despite temporally uninformative (i.e., early or late) feedback. For neuroimaging, we observed a dissociation between estimating and reproducing time intervals. Estimation engaged the default mode network (DMN), including the superior frontal gyri, precuneus, and posterior cingulate, whereas reproduction activated regions associated traditionally with the "timing network" (TN), including the supplementary motor area (SMA), precentral gyrus, and right supramarginal gyrus. Notably, greater and more extensive DMN involvement was observed in re-do trials, whereas for the TN, it was more constrained. Task-based connectivity between these networks demonstrated higher inter-network correlation primarily when estimating initial trials, while re-do trial communication was higher during reproduction. Overall, these results suggest that the DMN and TN jointly mediate subjective self-awareness to improve timing performance.

Significance Statement

A finely tuned sense of time perception is imperative for everyday motor actions (e.g., hitting a baseball). Timing self-regulation requires correct assessment and updating duration estimates if necessary. Using a modified version of a classical task of time measurement, we explored the neural regions involved in error detection, time awareness, and learning to time. Reinforcing the role of the SMA in measuring temporal information and providing evidence of co-activation with the default mode network, this study demonstrates that the brain overlays sensorimotor timing with a metacognitive awareness of its passage.

Introduction

When learning a new task (e.g., temporal processing of interval duration) or conducting a motor movement, humans must excel at initial self-assessment and update their actions if necessary. The brain's performance monitoring system detects errors as the motor program is performed and responds by sending a cognitive control signal to resolve the error, all without external feedback (Ullsperger et al., 2014). This compensatory process requires a degree of self-awareness of one's cognitive state or metacognition (Fleming et al., 2012; Shea et al., 2014). Furthermore, an awareness of the subjective passage of time and the ability to self-assess one's timing ability without prior sensory input require error-tracking mechanisms (Kononowicz and van Wassenhove, 2019).

Error correction is also a critical component of sensorimotor synchronization (SMS) tasks that comprise tapping in sync with an internal or external beat or rhythm (Repp and Su, 2013). This mechanism is observed in both audio and visual (SMS) studies in both humans and monkeys (Comstock et al., 2018) when adjusting timing movement to match changes in tempo in a beat-based task (Gámez et al., 2018). Typically, the error introduced in these experiments involves a shift in phase, period, or nonlinear behaviors (Bavassi et al., 2013), with the change in periodicity reaching the level of conscious awareness (Comstock et al., 2018).

Received May 22, 2023; revised Nov. 3, 2023; accepted Dec. 13, 2023.
Author contributions: F.B. and M.W. designed research; F.B. performed research; F.B. and M.W. analyzed data; F.B. wrote the first draft of the paper; F.B. and M.W. edited the paper; F.B. and M.W. wrote the paper.
The authors declare no competing financial interests.
Correspondence should be addressed to Martin Wiener at mwiener@gmu.edu.
https://doi.org/10.1523/JNEUROSCI.1789-22.2023

When extended to the sphere of learning and adapting to temporal intervals, robust systems for both error monitoring and metacognition are vital. Past behavioral and electrophysiological evidence confirm that humans are cognitively aware of timing errors; however, questions remain concerning the extent of this time awareness (Akdoğan and Balcı, 2017; Kononowicz and van Wassenhove, 2019; Riemer et al., 2019). A recent study demonstrates that when asked to either accept or reject a trial depending on the subjective perception of proximity to the target duration interval, participants are more likely to opt out of a trial when the match (distance) between the target and reproduced time interval is lower; reduced precision in timing behavior is also observed in these trials, again supplying evidence for this self-monitoring ability (Yallak and Balcı, 2022).

Are humans aware of the direction of their timing errors (earliness or lateness) or is this cognizance limited to only error magnitude? Furthermore, how does the process of learning to time impact this awareness? Previously, we tested participants on a classical test of time reproduction, the visual time reproduction task, and incorporated feedback that did not provide information about direction (earliness or lateness) and compared it to a condition with an absence of feedback (Bader and Wiener, 2021). We demonstrated that temporal estimates were more accurate and precise with post-trial non-directional feedback as participants learned and adapted to the time intervals (Bader and Wiener, 2021). Non-directional feedback was used because we were interested in understanding the limits of internal metacognitive processes associated with time perception, and evaluative ability to self-assess one's own timing aptitude, focusing on our capacity to detect lateness or earliness (error direction). Various conflicting studies have claimed that we have an awareness of directional and magnitude information while other experiments demonstrated that directional information is not intrinsically available (Akdoğan and Balcı, 2017; Riemer et al., 2019). Furthermore, in many instances, error representation has frequently failed to capture directional content.

Our present neuroimaging study tested the neural basis of this metacognitive ability with human participants of both sexes undergoing fMRI while they performed a visual temporal reproduction task with randomized supra-second intervals (1.5–6 s). Crucially, each trial was repeated following feedback, allowing a "re-do" to learn from the successes or errors in the initial trial. We hypothesized that traditional time perception networks would display BOLD activation parallel to a meta-analysis of 114 human experiments performing time measurement tasks while undergoing scanning (Cona et al., 2021). The most prominent of these areas is the supplementary motor area (SMA), deemed to be the accumulator in clock time models. Other regions associated with time representation include the inferior parietal lobe [containing the supramarginal gyrus (SMG)], the inferior frontal gyrus, thalamus, basal ganglia, and superior temporal gyrus (Cona et al., 2021) as well as the pre-SMA and bilateral insula (Naghibi et al., 2023).

We further hypothesized that the timing self-awareness aspect of our task may also engage the default mode network (DMN). Interactions between the timing network (TN) and default-mode-related activations are more pronounced with longer supra-second intervals (Morillon et al., 2009) and could relate to mentalizing interval durations. Specifically, the posterior cingulate and the precuneus are highly implicated in self-awareness of timing (Utevsky et al., 2014; Ustun et al., 2017).

Materials and Methods

Participants. Twenty-seven neurologically healthy, right-handed subjects were recruited for a simultaneous fMRI-EEG experiment. EEG event markers failed to load for all stages of the task for three subjects, thus leading to missing and insufficient trial counts. Another subject was unable to complete the entirety of the temporal reproduction task inside the scanner. The final data analysis included 23 right-handed neurologically healthy subjects (average age 23.17 ± 4.58 SD years, 12 males, 11 females). No significant differences were observed between the ages of males (24.5 ± 5.485) or females (21.636 ± 2.838) according to an independent *t*-test ($t = 1.595$, $df = 21$, $p = 0.126$).

Task. The task was delivered via Psychopy (www.psychopy.org) from a PC desktop in the MRI console room and projected to Cambridge Research Systems BOLD Screen 32 in. 1,920 × 1,080 resolution (120 Hz refresh rate) screen situated ∼1.5 m outside of the MRI bore. The task structure of the temporal reproduction task was composed of three phases: estimation, reproduction, and feedback for all three experiments (Fig. 1). These three phases were performed twice for each duration (Bader and Wiener, 2021). Each trial was initiated with a centrally presented fixation cross for a randomly presented duration of 2–6 s, drawn from a uniform distribution. In the estimation phase, a blue square was visually shown to the participant for one of five logarithmically spaced, randomly presented intervals (1.5–6 s). Until the square was on-screen, the participant was instructed to encode the duration in memory and to not use counting as a method to determine the elapsed time, which has been demonstrated as an effective means of eliminating counting strategies (Rattat and Droit-Volet, 2012). Following the estimation phase, there was a 4- to 8-s gap prior to the reproduction phase, drawn from a uniform distribution. Then, the blue square reappeared on-screen in the reproduction phase and the participant was asked to press a key on an MR-compatible handheld button box (Current Designs) when the blue square had remained on-screen for the same time duration as the time elapsed in the estimation phase. The subjects' button-press caused the square to disappear, signaling interval termination.

After every trial, adaptive feedback (duration = 1 s) was delivered 2–4 s after the disappearance of the square and informed the participant whether the response was on-target or off-target; notably, this feedback provided no index of the temporal direction of the error (i.e., early or late). On each trial, a feedback constant (k), starting with an initial value of 3.5, was adjusted such that the reproduced interval had to be within the range [interval/k] and was updated according to the 1-up/1-down rule with a step size of 0.015 which was either added or subtracted (Jazayeri and Shadlen, 2010). If the participant's reproduced interval was either 0.015 above or below the target duration, on-target feedback would be delivered; otherwise, off-target feedback was delivered. Critically, after each complete trial, participants had a second opportunity (the re-do trial) to perform the entire sequence of phases (estimation, reproduction, and feedback) again, ensuring feedback was applied to the appropriate duration. Participants were informed prior to the beginning of the experiment that they would have two opportunities (an initial and a re-do trial) to time the visual stimulus (blue square) which would be of the same duration in both types of trials. Subjects were able to distinguish the initial from the re-do because in the re-do trials, the text would read "Estimate-again" and "Reproduce-again." After the feedback on the re-do trial, subjects experienced a random delay drawn from an exponential distribution with a minimum duration of 3s before starting the next full trial (initial and re-do). In total, the experiment had 120 trials (10 durations/block × 6 blocks × 2 trials, initial and re-do). Participants were given a break after each block for a total of six blocks.

fMRI acquisition. A Siemens Magnetom 3T whole-body MR scanner was used to acquire all imaging sequences. First, a localizer was performed to identify the brain's position in space followed by a field map to measure the magnetic field inhomogeneity. Field mapping parameters were echo time (TE1) = 4.92 ms and TE2 = 7.38 ms, repetition time (TR)

= 731 ms, field-of-view (FOV) = 208 mm, matrix (104 × 104) voxel size = 2×2 × 2 mm, and 72 slices were collected with a 2 mm thickness. Next, a structural magnetization-prepared gradient-echo-planar image (MP-RAGE) T1* was performed with the following values: TR = 2,300, echo time (TE) = 2.23 ms, flip angle 8 degrees, FOV = 256 mm, matrix (256 × 256) 192 slices at a thickness of 0.88 mm were acquired with MP-RAGE sequence. Echo-planar image (EPI) T2* scans were then collected with the following parameters (TR = 2,390 ms, TE = 30 ms, 90-degree flip angle, FOV = 192 mm, and matrix = 94 × 94). Forty interleaved slices with a transverse orientation, a slice thickness of 3 mm, and 3 × 3 × 3 mm voxel size were taken. Each participant underwent one localizer, one field map, one MP-RAGE, and six BOLD EPI sessions.

fMRI pre-processing steps. All pre-processing steps were performed in SPM 12 on 3D nifti files generated from the MP-RAGE, field map, and the six EPI T2 sequences. First, voxel displacement was calculated using the magnitude and phase images from the field map, followed by a slice timing correction, realignment, and calculation of six affine rigid movement parameters related to head movement and unwarping. Images were then normalized to standard Montreal Neurological Institute (MNI) anatomical space and mean BOLD values were computed, written, and smoothed with a 6 mm^3 Gaussian kernel. Behavioral data on onset times and durations for each of the various phases (estimation, reproduction, and feedback) in both the initial and re-do trials were extracted and loaded by an in-house batch processing Matlab script which then estimated and wrote a first-order general linear model (GLM) for each individual participant using the BOLD images; individual events were time-locked to the start of estimation and reproduction phases for initial and re-do trials, separately, by convolving the canonical hemodynamic response (HDR) function with a boxcar stretched to match the duration of either the presented or reproduced interval on each trial (Mumford et al., 2023).

This event-related experimental design incorporated jittering to enable the full HDR to evolve with the shortest duration (1.2 s) in this experiment (Mumford et al., 2023). Visual stimulation studies have illustrated that the BOLD response, while nonlinear, is able to be detected at stimulus durations as low as 5 ms and that the initial "dip" due to cerebral metabolic rate may be colocalized with the positive BOLD response (Yeşilyurt et al., 2008). Next, SPM's contrast manager was used to create contrasts to examine changes in BOLD activation between the task phases and between the initial and re-do trials of those phases in this combined dataset. The specified contrasts and weights were then fed into an additional in-house Matlab script and a second-level group GLM was estimated and written. Afterward, in SPM, one-sample *t*-tests were performed for each contrast and whole brain group level results were displayed with a voxelwise threshold of $p < 0.001$, uncorrected and a cluster threshold of $p < 0.05$, familywise error corrected.

Statistics. Jeffreys' Amazing Statistics Program (JASP) 0.16 (JASP team, 2021) was used to analyze the behavioral data from the temporal reproduction task. The data were normally distributed and passed the Shapiro–Wilks test of normality for the proportional temporal error, accuracy, and precision [as measured by the coefficient of variation (CV)]. Proportional temporal error was calculated as the reproduced duration minus the target duration divided by the target duration. The CVs were calculated as the standard deviation of the reproduced durations divided by the participant's mean reproduced durations and two separate CV values were generated for the initial and re-do trials. The slope was calculated from a regression line of the mean reproduced durations (*y*-values)/aggregated average of the sample target durations (*x*-values). Two slope values representing the initial and re-do slopes were generated. In-house Matlab scripts were written to examine re-do slope performance based on initial trial slopes associated with on- or off-target feedback.

A linear mixed effects model of proportional error [fixed effects: target duration, trial type (initial vs re-do), random effects: subjects] was used to detect changes between initial and re-do trials. Outlier values that were three median absolute deviations from the median were removed using the Matlab function *isoutlier*. We chose this measure, as opposed to the mean, as it is more robust when dealing with skewed distributions (Leys et al., 2013), as are often observed in reaction time and time reproduction experiments (Rousselet and Wilcox, 2018).

Functional connectivity. To further explore putative interactions between the DMN and regions involved in time perception, we conducted an additional functional connectivity analysis. To accomplish this, we began by taking a beta-series approach, wherein single-subject GLMs were reconstructed for each subject as described above, with the exception that each trial was modeled as a separate covariate. The resulting GLM thus generated a time-series of beta values for each trial type (initial and re-do) and phase (estimation and reproduction). Next, beta-series were averaged across a series of regions of interest (ROIs). For the DMN, these regions were derived from the Yeo atlas, accessible at https://surfer.nmr.mgh.harvard.edu/fswiki/CorticalParcellation_Yeo2011, and consisted of 12 regions including the bilateral posterior cingulate cortex, superior frontal gyrus, angular gyrus, precuneus, anterior cingulate cortex, and middle temporal gyrus. All ROIs were constructed from the automatic anatomic labeling atlas definitions. For time perception, we relied on a series of regions derived from several neuroimaging meta-analyses and recently synthesized into a series of 17 ROIs, accessible at https://neurovault.org/collections/13081/ (Fig. 2). These regions, now referred to as the TN, include the bilateral frontal operculum, SMA, insula, inferior parietal lobe, caudate, putamen, cerebellum (dentate gyrus), and thalamus, as well as the left precentral gyrus, right pars triangularis, and SMG. We used brain regions from pre-defined atlas ROIs rather than univariate contrast-derived ROIs for the connectivity analysis because we did not want to exclude brain regions commonly observed across other studies in these networks (namely, the DMN and TN) that were not observed in the present study. Additionally, by using these atlases for the connectivity analysis, we hope to enable better replication of our results in future work.

To explore connectivity between these regions and how they might change across task conditions, we first calculated Spearman correlation matrices for the beta-series from all 29 ROIs, across the 4 task conditions; this analysis thus yielded both inter- and intra-network connectivity measures between DMN and TN regions. The Spearman correlation coefficient was chosen to reduce possible confounds driven by possible outlier trials within the beta-series. Next, to compare correlation matrices, we converted Spearman correlations to *z*-scores using Fisher's r-to-z tranform. Lastly, paired *t*-tests were conducted comparing *z*-scores from each of the conditions in a 2 × 2 design. To assess significance, *p*-values were further corrected for multiple comparisons using the false-discovery rate (FDR) algorithm to a corrected value of $p < 0.05$.

Results

A linear mixed effects model with trial type (initial and re-do) as a fixed effect and subject as a random effect and model terms nested with the Satterthwaite method, performed on the proportional temporal error, defined as the relative difference between reproduced and actual time interval, exhibited a significant effect of duration [$F(1, 2719.04) = 248.362$, $p < 0.001$] and trial type [$F(1, 2719.01) = 12.795$, $p < 0.001$], but no interaction [$F(1, 2718.01) = 1.106$, $p = 0.293$], suggesting that the change in error did not differ across durations. Fixed effects estimates demonstrated a reduction in error on re-do trials compared to initial ones [$\beta = 0.017$, SE = 0.005] such that timing performance improved when provided a second chance (Fig. 1). Estimated marginal means from the linear mixed model, with degrees of freedom estimated using the Satterthwaite method, further demonstrated that the proportional error on initial trials was significantly different than zero [mean: −0.049, 95% CI: −0.095 to −0.003, $t(24.135) = -2.214$, $p = 0.037$], whereas for re-do trials, it was not [mean: −0.015, 95% CI: −0.061 to 0.031; $t(24.135) = -0.693$, $p = 0.495$], demonstrating an improvement in performance.

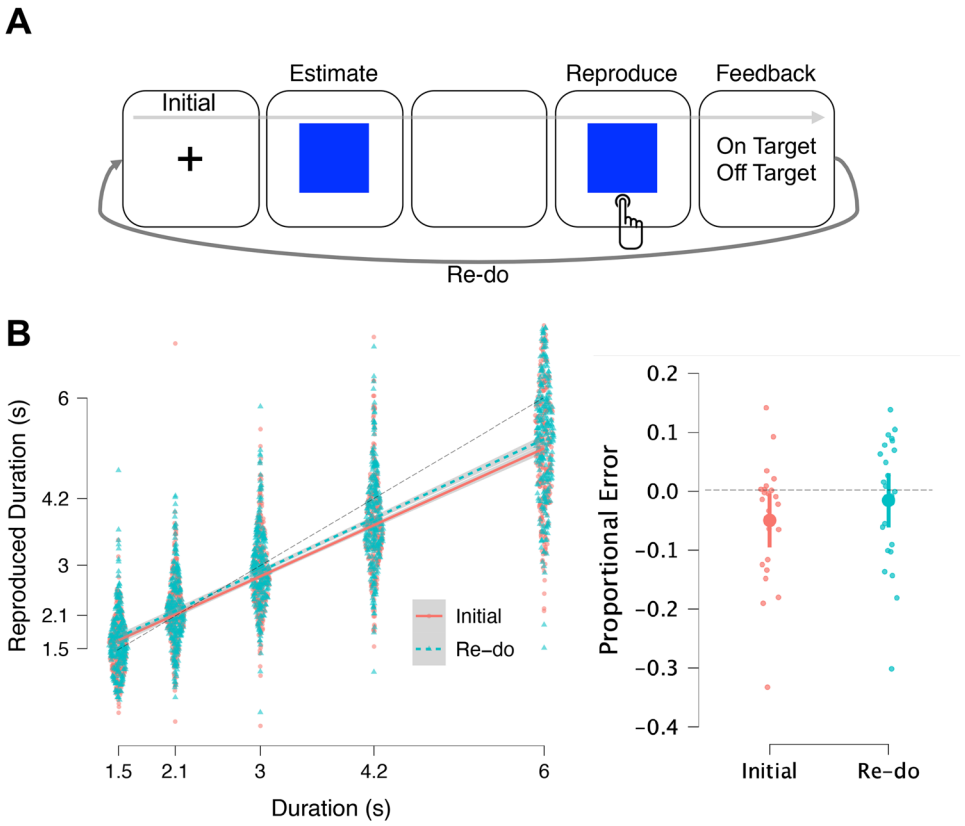

Figure 1. Task and data. ***A***, Task schematic for the time reproduction task. On initial trials, subjects were presented with a blue square for a randomly chosen interval of time, consisting of the estimate phase. A second blue square was presented at the start of the reproduction phase, in which subjects were required to press a response button to terminate the interval so that it matched the one just shown. Non-directional feedback was then presented, depending on whether the reproduced interval landed within an adaptive range of the presented interval. Following this, subjects were given a "re-do" trial, on which they could repeat the entire sequence again. ***B***, Behavioral data. Left panel displays individual performance from all subjects for each of the presented durations (1.5–6 s), in which Re-do trial performance shifted closer to the expected durations; dashed line indicates the identity, where perfect performance would lie. Right panel displays the estimated marginal means for signed proportional error between initial and re-do trials; dashed line indicates zero error, where perfect performance would lie. Error bars represent 95% confidence intervals.

A repeated measures ANOVA on mean reproduced intervals revealed that the participants' reproduced durations for the re-do trials shifted closer to the identity line and the target durations in a directionally appropriate way when compared to the initial trial [F (1, 22) = 14.146, $p < 0.001$], again showing an improvement in temporal estimates (Fig. 1). Participants, however, did not display significantly better precision (lower CV) in their re-do trials [F (1, 1.562), $p < 0.225$], but did exhibit a main effect of duration [F (4, 26.239), $p < 0.001$].

We also investigated the re-do trial reproduced durations, CVs, initial and re-do slopes, and slopes based on the initial trial feedback (on/off) by separating the re-do trial estimates according to whether the initial trial was on- or off-target. No significant differences were observed for the reproduced durations and CVs (all $p > 0.05$). The initial trial slopes (0.768 ± 0.127) and re-do trial (0.793 ± 0.126) were not significantly different from one another according to a paired t-test: $t(22) = -1.497$, $p = 0.149$, CI: −0.728 to −0.110. However, a deeper dissection of when the re-do trial slope was preceded by on-target feedback in the initial trial revealed that it was significantly different than when the initial trial was off-target, illustrating that estimates were more certain and closer to the identity line in the on-target condition $t(22) = 2.69$, CI: 0.007 ± 0.16, $p = 0.033$; on-target slope = 0.828, off-target slope = 0.745. Our previous behavior-only study had similar findings and showed individual re-do slopes varying significantly between on- and off-feedback in the initial trials and showing more certainty with initial on-target feedback (Bader and Wiener, 2021).

Imaging results

Estimation initial—reproduction initial contrast

BOLD activations were seen in the bilateral superior frontal gyrus, right middle frontal gyrus, left angular and SMG, left middle occipital gyrus, right post- and precentral gyrus, bilateral precuneus, and posterior cingulate gyrus. In this inter-phase contrast, more parietal involvement for time perception (angular gyrus and SMG) along with precentral gyrus for motor movement was observed in conjunction with the recruitment of structures associated with the DMN (posterior cingulate gyrus) and metacognition (precuneus) (Fig. 2 and Table 1).

Reproduction initial—estimation initial contrast

Significant activations were observed in the left pre- and postcentral gyrus, bilateral SMA, bilateral middle cingulate gyrus, bilateral superior frontal gyrus, left central operculum, left parietal operculum, left SMG, right occipital pole, right cuneus, right calcarine and lingual cortex, and superior occipital gyrus. The SMA is recruited again when re-creating the interval duration jointly with timing-related, parietal brain areas to include the SMG, left central, and parietal operculum. High detection of activity in the superior frontal gyrus also reiterates that the brain's performance monitoring system is online. Visual processing of the

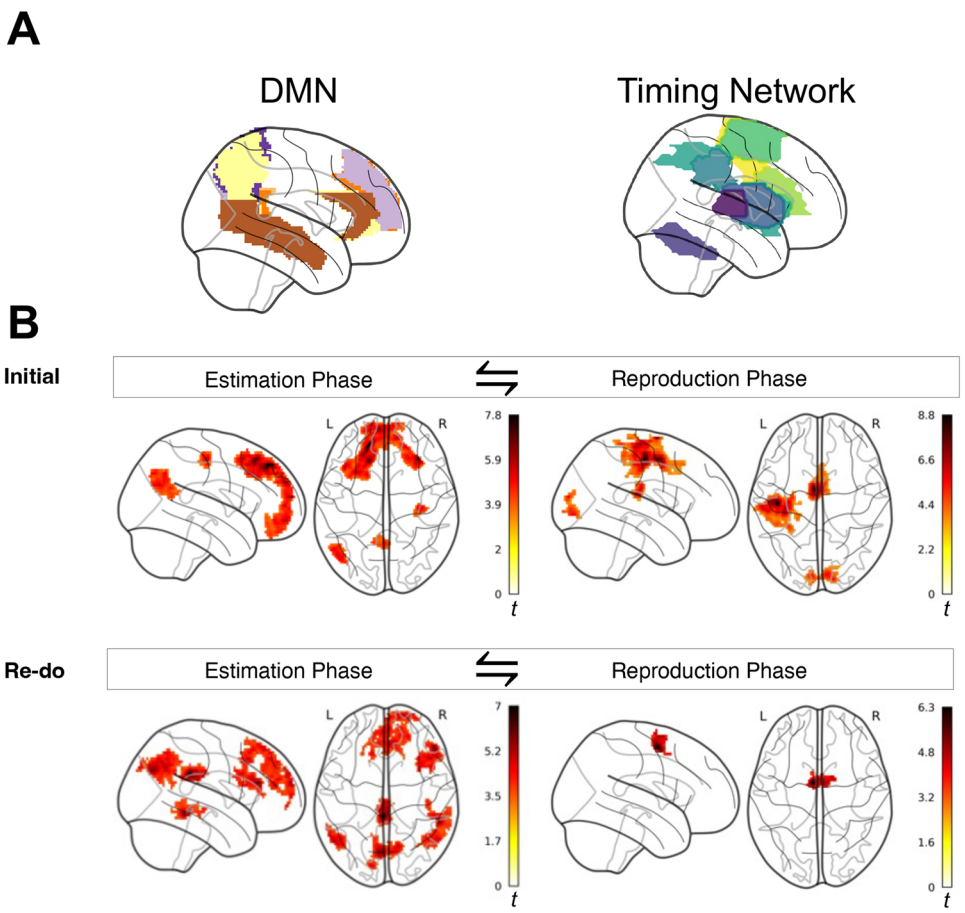

Figure 2. Neuroimaging results. ***A***, Example ROIs for the DMN and the TN are displayed. ***B***, The top panel displays the contrast between estimation and reproduction phases on initial trials. Here, the estimation phase invoked greater activity in DMN regions, including the superior frontal gyri, precuneus, and ACC. For the reproduction phase, activation was instead observed in the TN, including the SMA and left precentral gyrus, as well as the occipital cortex. The bottom panel displays the same contrast, but for the re-do trials. DMN activation was again observed for the estimation phase, but more widespread, whereas TN activation was more constrained, with only the SMA exhibiting significant activation. All displayed maps were thresholded at $p < 0.001$, uncorrected voxelwise, and $p < 0.05$, FWE corrected at the cluster level.

stimuli is emphasized again due to the eliciting of the BOLD signal in the occipital lobe.

Estimation re-do—reproduction re-do contrast
Task-related activations were witnessed in the right frontal pole, bilateral superior frontal gyrus medial segment, anterior cingulate cortex, right superior frontal gyrus, right middle frontal gyrus, right triangular and opercular part of the inferior frontal gyrus, right precentral gyrus, left superior occipital gyrus, right inferior temporal gyrus, right middle and superior temporal gyri, left cuneus and bilateral middle cingulate gyrus, bilateral precuneus and posterior cingulate, bilateral angular gyrus, and left SMG. Regions related to forming duration judgements (inferior frontal gyrus, bilateral angular gyrus, and SMG) along with self-awareness (precuneus) and the DMN (posterior cingulate cortex) have high BOLD activation when comparing the re-do trials between phases (Fig. 2 and Table 2).

Reproduction re-do—estimation re-do contrast
BOLD activations were seen in the bilateral SMA and the right superior frontal gyrus, in conjunction with invoking the brain's performance monitoring system (superior frontal gyrus).

Estimate initial–estimate re-do contrast
No suprathreshold clusters in the fMRI peak activations for the estimate initial–estimate re-do contrast were observed.

Estimate re-do—estimate initial contrast
The fMRI peak activations for the contrast estimate re-do–estimate initial displayed high BOLD activations in the bilateral calcarine cortex, bilateral lingual gyrus, left cuneus, left occipital pole, and the left occipital fusiform gyrus (Table 3). These are all visual processing areas and indicate that the subject is observing and fixating on the blue square in order to encode it.

Reproduce initial–reproduce re-do
Neural activations in the reproduce initial–reproduce re-do contrasts were detected in the calcarine cortex, the exterior cerebellum, bilateral SMA (mainly right hemisphere), right superior frontal gyrus, the right anterior cingulate gyrus, left postcentral gyrus, left SMG, right calcarine cortex, bilateral thalamus, posterior insula, bilateral caudate, right putamen, right hippocampus, right posterior insula, right pallidum, and right accumbens (Fig. 3 and Table 4). Here, in addition to time perception related areas (SMA, SMG, and basal ganglia) and interoceptive awareness (insula), activation was observed in memory-related regions (hippocampus) as the encoded time is recalled and performance is monitored (superior frontal gyrus and anterior cingulate cortex) when decisions about the duration are made in the initial and re-do trials. Notably, activation was also exhibited in the cerebellum, a region that has been associated with error learning. Previously, higher cerebellar activity has been viewed in fMRI

Table 1. Estimate—reproduce for initial trials

Contrast condition	Location	Hemisphere	*x*	*y*	*z*	*t*-Score	Cluster size
$Estimate_{initial}$ − $Reproduce_{initial}$	Superior frontal gyrus	L	−18	43	47	7.82	2,353
	Middle frontal gyrus	R	33	29	53	6.72	
	Superior frontal gyrus	R					
	Angular gyrus	L	−53	−61	38	5.28	276
	SMG	L					
	Middle occipital gyrus	L	−49	−67	26	5.26	
	Precentral gyrus	R	35	−20	53	5.70	118
	Postcentral gyrus	R					
	Precuneus	R,L	0	−55	23	4.72	129
	Posterior cingulate gyrus	R,L					
$Reproduce_{initial}$ − $Estimate_{initial}$	Precentral gyrus	L	−40	−16	53	8.85	1,083
	Postcentral gyrus	L					
	Supplementary motor area	L	−4	−2	53	7.96	588
	Middle cingulate	L, R					
	Superior frontal gyrus	L	−6	−4	74	7.16	
	Superior frontal gyrus	R	6	−2	74	4.82	
	Supplementary area	R					
	Occipital pole	R	15	−92	14		225
	Cuneus	R					
	Calcarine cortex	R					
	Superior occipital gyrus	R					
	Lingual gyrus	R	9	−87	−4		
	Central operculum	L	−57	−20	20		154
	Calcarine cortex	R					
	Postcentral gyrus	L					
	Parietal operculum	L					
	SMG	L					

MNI coordinates are provided for all cluster peaks and sub-peaks. Brain regions lacking coordinates represent single-peak clusters overlapping multiple areas.
The brain regions with peak coordinates and no cluster size values are sub-peaks within the same cluster.

Table 2. Estimate—reproduce for re-do trials

Contrast condition	Location	Hemisphere	*x*	*y*	*z*	*t*-Score	Cluster size
$Estimate_{re\text{-}do}$ − $Reproduce_{re\text{-}do}$	Frontal pole	R	15	66	17	5.39	971
	Superior frontal gyrus medial segment	L,R	−2	49	17	5.01	
	Anterior cingulate gyrus	L,R					
	Superior frontal gyrus	R	9	39	53	4.98	
	Middle frontal gyrus	R	49	31	22	6.13	453
	Triangular part of the inferior frontal gyrus	R					
	Opercular part of the inferior frontal gyrus	R	45	13	26	4.94	
	Precentral gyrus	R					
	Precuneus	L	−6	−73	32	6.02	432
	Superior occipital gyrus	L	−14	87	35	4.89	
	Cuneus	L					
	Precuneus	R	13	−67	44	4.85	
	Posterior cingulate	L, R	−2	−36	29	7	297
	Middle cingulate gyrus	R,L	0	−28	23	5.31	
	Precuneus	R,L	2	−45	35	3.69	
	Angular gyrus	R	53	−61	38	4.74	296
	Middle occipital gyrus	R	43	−65	26	4.33	
	Angular gyrus	L	−51	−61	35	5.36	255
	SMG	L	−55	−53	44	4.31	
	Inferior temporal gyrus	R	56	−43	−13	6.08	253
	Middle temporal gyrus	R	47	−36	−7	4.89	
	Superior temporal gyrus	R	43	−22	−7	4.41	
$Reproduce_{re\text{-}do}$ − $Estimate_{re\text{-}do}$	Supplementary motor area	L	−6	−2	56	6.34	261
	Supplementary motor area	R	4	−2	56	6.34	
	Superior frontal gyrus	R	15	2	68	4.90	

MNI coordinates are provided for all cluster peaks and sub-peaks. Brain regions lacking coordinates represent single-peak clusters overlapping multiple areas.

studies in trials with sensory errors than trials without errors (Diedrichson et al., 2005; Schlerf et al., 2012). The cerebellum also plays a role in performance monitoring, error processing, and feedback learning (Peterburs and Desmond, 2016) in conjunction with predictive timing and the regulation of trial-by-trial variation in self-timing (Tanaka et al., 2020), particularly due to connections with the frontoparietal cortices (Tanaka et al., 2020).

Table 3. Estimate re-do–estimate initial

Contrast condition	Location	Hemisphere	*x*	*y*	*z*	*t*-Score	Cluster size
Estimate{Re-do — Initial}	Calcarine cortex	L,R	−2	−92	−4	5.45	116
	Lingual gyrus	L,R					
	Cuneus	L					
	Occipital pole	L					
	Lingual gyrus	L	−12	−83	−7	4.96	
	Occipital fusiform gyrus	L					

MNI coordinates are provided for all cluster peaks and sub-peaks. Brain regions lacking coordinates represent single-peak clusters overlapping multiple areas.

Table 4. Initial–re-do for reproduction phase

Contrast condition	Location	Hemisphere	*x*	*y*	*z*	*t*-Score	Cluster size
Reproduce{Initial — Re-do}	Calcarine cortex	R	19	−71	8	6.13	1,228
	Cerebellum exterior	R	19	−59	−16	5.67	
	Supplementary motor cortex	R, L	4	27	56	6.88	363
	Superior frontal gyrus	R					
	Superior frontal gyrus medial segment	R, L	0	37	32	5.34	
	Anterior cingulate gyrus	R	4	29	35	5.17	
	Caudate	R	9	4	−1	5.33	248
	Pallidum	R					
	Thalamus	R	9	−2	5	5.32	
	Accumbens area	R					
	Caudate	L	−10	−2	20	4.48	
	Thalamus	L					
	Hippocampus	R	33	−24	−4	5.50	108
	Putamen	R					
	Posterior insula	R					
	Thalamus	L	−22	−22	14	6.04	85
	Postcentral gyrus	L	−55	−26	50	6.37	84
	SMG	L					
Reproduce{Re-do — Initial}	Medial frontal cortex	L, R	−2	47	−16	5.07	107
	Gyrus rectus	L					
	Medial frontal cortex	L, R	−2	58	−7	4.43	
	Superior frontal gyrus medial segment	L, R					
	Gyrus rectus	L, R	−2	45	−25	3.78	
	Medial orbital gyrus	L					

MNI coordinates are provided for all cluster peaks and sub-peaks. Brain regions lacking coordinates represent single-peak clusters overlapping multiple areas.

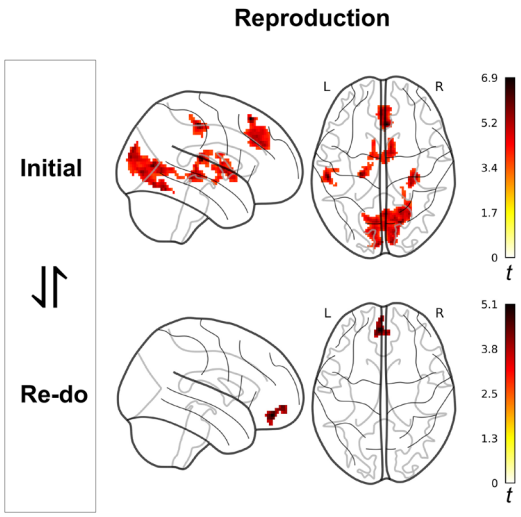

Figure 3. Comparisons between reproduction phase initial and re-do trials. Here, significant differences were only observed during the reproduction phase, in which the SMA, ACC, basal ganglia, and right hippocampus were active, whereas on re-do trials, only the medial orbitofrontal cortex was active.

Reproduce re-do–reproduce initial contrast

No significant activation was observed using our threshold. However, using a lower threshold of $p < 0.001$, uncorrected with a cluster extend of $k = 10$ found task-related BOLD activations in the bilateral medial frontal cortex, bilateral gyrus rectus, bilateral superior frontal gyrus medial segment, and the left medial orbital gyrus. Recruitment of brain regions in performance monitoring (medial frontal cortex) and working memory (superior frontal gyrus) (Alagapan et al., 2019) are displayed in the reproduction phase, demonstrating a mechanism for error detection and correction.

Functional connectivity

Interconnectivity patterns

The functional connectivity analysis revealed a double-dissociation between task phase (estimation and reproduction) and trial type (initial and re-do). Broadly, we observed that connectivity between the DMN and TN was greater in the estimation phase, but more so on initial trials than re-do, whereas in the reproduction phase, inter-network connectivity was higher on re-do trials than initial ones (Fig. 4). More specifically, in the estimation phase, connectivity increased between the bilateral superior frontal gyrus and ACC of the DMN and the cerebellum, left caudate and insula, inferior frontal gyrus, and left precentral

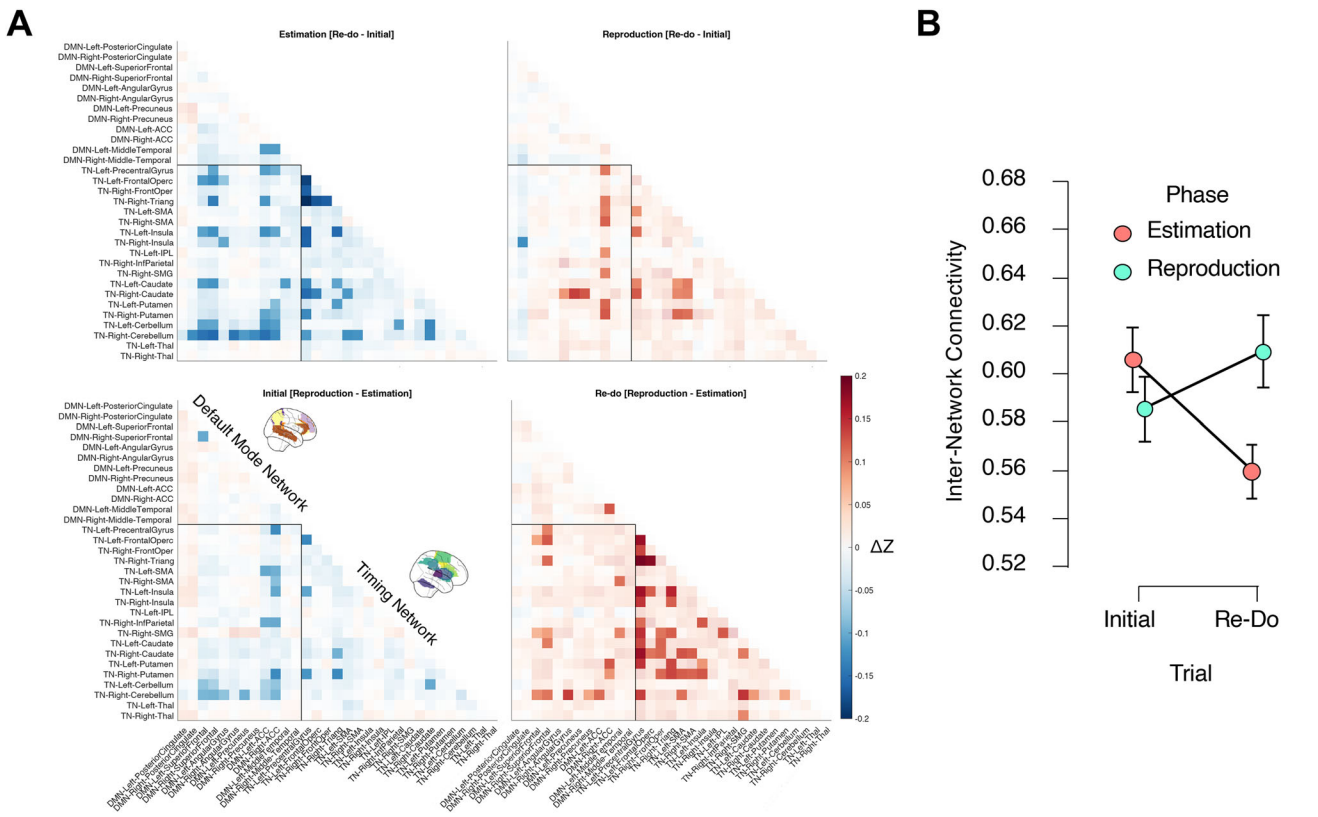

Figure 4. Functional connectivity results. ***A***, A double-dissociation was observed across phases (estimation vs reproduction) and trials (initial vs re-do) for inter-network connectivity between the DMN and TN, demarcated by the black rectangle in each panel. Here, greater connectivity was observed between the DMN and TN during the estimation phase, but primarily on initial trials, rather than re-do. In contrast, during the reproduction phase, greater inter-network connectivity was observed primarily on re-do trials. Pixel values represent the mean difference score between conditions; non-faded pixels indicate significant differences corrected for multiple comparisons with FDR to $p < 0.05$. ***B***, Same results from panel *A*, but displaying the average *Z*-score for inter-network connectivity, demonstrating a double-dissociation. Error bars represent standard error.

gyrus of the TN; notably, the right cerebellum exhibited the largest connectivity with the DMN across a variety of structures including the angular gyrus and precuneus. In contrast, in the reproduction phase, connectivity increased between the precuneus and the right caudate, as well as the right ACC and a variety of TN structures including the SMA, right SMG, and putamen. Finally, connectivity again increased between the superior frontal gyrus (SFG) and the cerebellum, caudate, and inferior frontal gyrus.

Intra-connectivity patterns

Greater intra-connectivity within the TN in the reproduction phase was observed in the re-do trials when compared to the initial trials. Increased connectivity was witnessed between the right putamen and right caudate with the bilateral SMA. Furthermore, in re-do reproduction trials, intra-connectivity within the TN was higher in the reproduction phase rather than the estimation phase. Specifically, the left precentral gyrus, right pars triangularis, and the bilateral frontal operculum showed enhanced connectivity. The right pars triangularis showed larger connectivity with the left precentral gyrus, left frontal operculum, and the bilateral insula. Broad intra-TN connectivity was seen with the precentral gyrus and left putamen, bilateral caudate, right SMG, and bilateral inferior parietal lobes; the right putamen and the bilateral operculum, pars right triangularis, and bilateral SMA. Greater connectivity was also witnessed between the right cerebellum, right SMG, and left caudate; and the right SMG, right operculum, and right pars triangularis. Similarly to the interconnectivity, the intra-TN connectivity was greater in the initial estimation rather than re-do. The left precentral gyrus had connectivity with the bilateral operculum and right pars triangularis. The right pars triangularis connected with the left precentral gyrus and the bilateral operculum. Bilateral insulas and caudates showed intra-connectivity with the left precentral gyrus. The right caudate had increased connectivity with left precentral gyrus and left frontal operculum. Initial estimation trials also had increased connectivity between the cerebellum and SMA and the right caudate and the bilateral cerebellum.

For the DMN, we note that far less intra-network connectivity was observed, with the exception of greater connectivity between the left middle temporal gyrus and ACC, as well as right and left superior frontal gyri on initial estimation and between left middle temporal gyrus and ACC on re-do reproduction.

Discussion

Behavioral and electrophysiological evidence suggest that humans and rodents can monitor errors during timing behavior (Akdoğan and Balcı, 2017; Kononowicz et al., 2019; Kononowicz et al., 2022). Studies reveal that subjects are cognitively aware of the timing errors they make, particularly when learning to time interval durations, which happens rapidly and within one trial (Simen et al., 2011). Our previous behavioral study demonstrated that when allowed to "re-do" a trial, humans can incorporate non-directional feedback to improve timing estimates both in accuracy and in precision (Bader and Wiener, 2021). Novel in using a mixed range of interval durations rather than a single

duration, this experiment also showed that in the absence of feedback, the accuracy of time reproductions improved whereas the precision did not. These results revealed that humans are aware of the direction of their timing error, a capacity requiring metacognition. Feedback was used in a previous behavior-only study to make timing more precise (Bader and Wiener, 2021). However, in the current study, participants' immersion in a fMRI scanner environment and the discomfort arising from a cramped space in conjunction with a complicated EEG electrode application and set-up may have impeded temporal precision from being enhanced. Our current neuroimaging experiment was used to determine the neural regions underlying this improvement in timing estimation. Behaviorally, we replicated our previous finding, the absolute temporal error decreased, and the accuracy of the temporal estimates was improved with reproduced targets approaching their target durations.

Our imaging results reinforced the behavioral results but also reiterated the importance of the SMA in representing temporal information and measuring time, which has been demonstrated repeatedly in the time perception literature (Ferrandez et al., 2003; Coull et al., 2004; Pouthas et al., 2005; Macar et al., 2006). The SMA contains a chronotopic map with localized regions preferentially responding to specific durations along an antero-posterior gradient and exhibits duration tuning (Protopapa et al., 2019). As the duration is encoded during estimation, the SMA is initially recruited and invoked again in the re-do trials during reproduction. This finding is aligned with both the behavioral data and the sharpening of temporal responses as evidenced by the reduction of temporal errors and accuracy improvement in the second re-do trial.

A second focus of our study was on regions of the DMN. While studies of time perception rarely implicate the DMN, some work has suggested a link between the two. For instance, DMN activation has been shown to increase as subjects time progressively longer intervals (Morillon et al., 2009), and periodic motion expectation also engages the DMN (Carvalho et al., 2016). More recently, multivariate lesion-symptom mapping has linked impairments in time awareness (i.e., the awareness of time passing) to disruption in DMN nodes (Skye et al., 2022). These findings suggest that the DMN and TN are linked and informative to one another in the support of awareness and understanding of our sense of time. As a final note, the DMN and TN largely do not overlap (Menon, 2023).

Notably, our results demonstrated a dissociation between activation of the DMN and regions putatively involved in timing across the initial and re-do trial opportunities, as well as between task phases. Specifically, estimating a duration was more likely to invoke DMN regions, whereas reproducing a duration was more likely to invoke timing regions. This difference suggests that, when explicitly encoding a time interval into memory, subjects are actively aware of time's passage, yet when reproducing that interval, the motor system drives the transformation of that estimate into a timed action. In the context of improvements in performance, DMN regions were more widespread on the re-do trials than the initial ones; yet, TN regions were more constrained on re-do trials. Indeed, only the SMA was significantly active on the reproduction phase of re-do trials. Yet, when comparing activity directly between initial and re-do trials, the reproduction phase also invoked activity in the hippocampus initially and the medial orbitofrontal cortex on re-do trials. Altogether, the results suggest that DMN regions may serve to monitor timing performance and, when necessary, provide an update to motor system regions for the purpose of executing a precisely timed response.

One exception to the above findings is activation observed in the visual cortex and hippocampus during the reproduction phase. Both regions represent those outside commonly reported areas in explicit time perception, yet have both been reported to be important. For the visual cortex, previous work has shown linear increases in BOLD activation in this region in anticipation for an upcoming target (Bueti et al., 2010), as well as increases in neuronal firing rates of V1 neurons in mice (Shuler and Bear, 2006). Stimulation of this region has also been shown to disrupt timing performance, yet only when performed early within the interval (Salvioni et al., 2013), an effect which may rely on individual alpha frequency (Mioni et al., 2020). Curiously, visual cortex activity was only observed on the initial trials, and not on re-do, when timing performance improved. One possibility is that, on the initial trials, subject timing was partially driven by the exogenous visual cue, whereas on the re-do trials, this cue was more effectively ignored, allowing subjects to rely on an endogenous sensorimotor signal.

For the right hippocampus, this region was also observed primarily on the reproduction phase of initial trials, which may be due to subjects retrieving the experienced cue from memory. Yet, this region was also less active on the re-do trials, when subject performance improved. One possibility here may relate to the so-called "central tendency" effects commonly observed in time reproduction tasks specifically (Jazayeri and Shadlen, 2010) and magnitude-based tasks more generally (Petzschner et al., 2015). In central tendency, subjects gravitate reproduced responses to the mean of the stimulus-set, an effect suggested to arise from reliance on a Bayesian prior in the face of timing uncertainty. Notably, the central-tendency effect is reduced on re-do trials (Bader and Wiener, 2021), which may be explained by subjects relying on a more precise representation of the perceived interval, and so less on the prior (Cicchini et al., 2012). Relatedly, on a distance reproduction task, similar in nature to this one, the right hippocampus has been shown to correlate with the degree of central tendency (Wiener et al., 2016), suggesting a similar effect may be at play here.

Our functional connectivity analysis also demonstrated a double-dissociation between phases and trial types, with internetwork communication between the DMN and the TN increasing more when estimating a time interval on initial trials and when reproducing one on re-do trials. One possible explanation for this difference is that on initial trials, subjects may already be aware of their error in their initial response, and so only require network cross-talk again when reproducing the interval on the re-do trial, when subject performance improved. An implication of this finding is that, if the DMN and TN were to become disconnected, subjects would exhibit no improvements in timing performance on re-do trials, and moreover would be unable to report how they had erred. Evidence for this dissociation comes from a study of patients with Parkinson's disease, who exhibited a difference in precuneus activation on a time reproduction task when tested on or off dopaminergic medication (Dušek et al., 2012).

With regard to specific regions, three nodes that exhibited the broadest connectivity patterns were the superior frontal gyrus and ACC of the DMN, and the cerebellum for the TN. Both the superior frontal gyrus and ACC have been implicated previously in performance monitoring studies. In particular, recent work in both humans and non-human primates have demonstrated that sensorimotor regions, particularly the SMA, lead connections with the ACC for the purpose of monitoring actions for errors (Bonini et al., 2014; Sarafyazd and Jazayeri, 2019; Fu et

al., 2022). For the cerebellum, a region long implicated in sensorimotor timing, connectivity with the DMN, was highest when encoding the stimulus duration. One aspect of this may relate to self-awareness of timing uncertainty as the interval is measured (Peterburs and Desmond, 2016). Indeed, recent work has suggested that the cerebellum serves to compute a Bayesian posterior estimate of duration (Narain et al., 2018).

We noted that the BOLD signal effect sizes related to the task epoch were also large. There are numerous explanations for this effect. A recent machine learning study revealed that neural networks estimate time through stereotyped neural trajectories in which the sensed elapsed interval is dependent on the final position of the trajectory. Temporal interval duration prediction was dependent on temporal scaling and attractor dynamics of the neural network converging for all durations (Bi and Zhou, 2020; Merchant and Perez, 2020) and has been witnessed in monkey medial frontal cortex recordings of different firing rates associated with different durations (Wang et al., 2018). Changed speed in response to the stimulus duration and temporal scaling have been associated with rodent time reproduction (Henke et al., 2021). Single duration timing is not only impacted; neuronal state space trajectories of beat-based, rhythmic timing also undergo amplitude modulation as durations are encoded (Gámez et al., 2019).

Research reveals that prior experiences with a particular duration influenced time perception as evidenced by different firing rates of primate PFC neurons based on varying prior experience with the duration. Computationally, this occurs through the warping of time representation via a manifold (Sohn et al., 2019). Finally, β power state space trajectories have been highly implicated in human time production studies for both producing the interval and self-judgment of timing performance with more distinct trajectories yielding better metacognitive judgments (Kononowicz et al., 2019).

Conclusion

Overall, this study underscores the importance of timing cognizance in improving timing performance. The recruitment of the DMN as the interval duration is encoded and perceived in the re-do signals this network's dual responsibility in tracking and adjusting to timing errors while a properly timed motor response is implemented in a situation with multiple opportunities (for example, hitting a baseball on the second try).

Finally, an understanding of how time awareness operates in the neurotypical brain can provide insights when timing is disrupted. In the case of autistic children, time reproduction accuracy and precision remained intact while the children were unable to evaluate their own timing ability (Doenyas et al., 2019). Due to the inter-network connectivity between the default mode and TNs, any disorder or injury that impacts the TN structures could also potentially adversely affect the DMN regions, leading to not only a distortion in temporal representation but also in its awareness.

References

Akdoğan B, Balcı F (2017) Are you early or late?: temporal error monitoring. J Exp Psychol Gen 146:347–361.

Alagapan S, Lustenberger C, Hadar E, Shin HW, Fröhlich F (2019) Low-frequency direct cortical stimulation of left superior frontal gyrus enhances working memory performance. Neuroimage 184:697–706.

Bader F, Wiener M (2021) Awareness of errors and feedback in human time estimation. Learn Mem 28:171–177.

Bavassi ML, Tagliazucchi E, Laje R (2013) Small perturbations in a finger-tapping task reveal inherent nonlinearities of the underlying error correction mechanism. Hum Mov Sci 32:21–47.

Bi Z, Zhou C (2020) Understanding the computation of time using neural network models. Proc Natl Acad Sci U S A 117:10530–10540.

Bonini F, Burle B, Liégeois-Chauvel C, Régis J, Chauvel P, Vidal F (2014) Action monitoring and medial frontal cortex: leading role of supplementary motor area. Science 343:888–891.

Bueti D, Bahrami B, Walsh V, Rees G (2010) Encoding of temporal probabilities in the human brain. J Neurosci 30:4343–4352.

Carvalho F, Chaim K, Sanchez T, Araujo D (2016) Time-perception network and default mode network are associated with temporal prediction in a periodic motion task. Front Hum Neurosci 10:1–13.

Cicchini GM, Arrighi R, Cecchetti L, Giusti M, Burr DC (2012) Optimal encoding of interval timing in expert percussionists. J Neurosci 32:1056–1060.

Comstock DC, Hove MJ, Balasubramaniam R (2018) Sensorimotor synchronization with auditory and visual modalities: behavioral and neural differences. Front Comput Neurosci 12:53.

Cona G, Wiener M, Scarpazza C (2021) From ATOM to GradiATOM: cortical gradients support time and space processing as revealed by a meta-analysis of neuroimaging studies. Neuroimage 224:117407.

Coull JT, Vidal F, Nazarian B, Macar F (2004) Functional anatomy of the attentional modulation of time estimation. Science (New York, N.Y.) 303:1506–1514.

Diedrichsen J, Hashambhoy Y, Rane T, Shadmehr R (2005) Neural correlates of reach errors. J Neurosci 25:9919–9950.

Doenyas C, Mutluer T, Genç E, Balcı F (2019) Error monitoring in decision-making and timing is disrupted in autism spectrum disorder. Autism Res 12:239–487.

Dušek P, Jech R, Sieger T, Vymazal J, Růžička E, Wackermann J, Mueller K (2012) Abnormal activity in the precuneus during time perception in Parkinson's disease: an fMRI study. PLoS One 7:e29635.

Ferrandez AM, Hugueville L, Lehéricy S, Poline JB, Marsault C, Pouthas V (2003) Basal ganglia and supplementary motor area subtend duration perception: an fMRI study. NeuroImage 19:1532–1576.

Fleming SM, Huijgen J, Dolan RJ (2012) Prefrontal contributions to metacognition in perceptual decision making. J Neurosci 32:6117–6125.

Fu Z, Beam D, Chung JM, Reed CM, Mamelak AN, Adolphs R, Rutishauser U (2022) The geometry of domain-general performance monitoring in the human medial frontal cortex. Science 376:eabm9922.

Gámez J, Mendoza G, Prado L, Betancourt A, Merchant H (2019) The amplitude in periodic neural state trajectories underlies the tempo of rhythmic tapping. PLoS Biol 17:e3000054.

Gámez J, Yc K, Ayala YA, Dotov D, Prado L, Merchant H (2018) Predictive rhythmic tapping to isochronous and tempo changing metronomes in the nonhuman primate. Ann N Y Acad Sci 1423:396–414.

Henke J, Bunk D, von WD, Häusler S, Flanagin VL, Thurley K (2021) Distributed coding of duration in rodent prefrontal cortex during time reproduction. Elife 10:1–24.

Jazayeri M, Shadlen MN (2010) Temporal context calibrates interval timing. Nat Neurosci 13:1020–1026.

Kononowicz TW, Roger C, van Wassenhove WV (2019) Temporal metacognition as the decoding of self-generated brain dynamics. Cereb Cortex 29:4366–4380.

Kononowicz TW, van Wassenhove V (2019) Evaluation of self-generated behavior: untangling metacognitive readout and error detection. J Cogn Neurosci 31:1641–1657.

Kononowicz TW, van Wassenhove V, Doyère V (2022) Rodents monitor their error in self-generated duration on a single trial basis. Proc Natl Acad Sci U S A 119:1–9.

Leys C, Ley C, Klein O, Bernard P, Licata L (2013) Detecting outliers: Do not use standard deviation around the mean, use absolute deviation around the median. J Exp Soc Psychol 49:764–766.

Macar F, Coull J, Vidal F (2006) The supplementary motor area in motor and perceptual time processing: fMRI studies. Cognitive processing 7:89–183.

Menon V (2023) 20 years of the default mode network: a review and synthesis. Neuron 111:2469–2487.

Merchant H, Perez O (2020) Estimating time with neural networks. Nat Mach Intell 2:492–493.

Mioni G, Shelp A, Stanfield-Wiswell CT, Gladhill KA, Bader F, Wiener M (2020) Modulation of individual alpha frequency with tACS shifts time perception. Cereb Cortex Commun 1:tgaa064.

Morillon B, Kell CA, Giraud AL (2009) Three stages and four neural systems in time estimation. J Neurosci 29:14803–14811.
Mumford JA, Bissett PG, Jones HM, Shim S, Rios JAH, Poldrack RA (2023) The response time paradox in functional magnetic resonance imaging analyses. Nat Hum Behav.
Naghibi N, Jahangiri N, Khosrowabadi R, Eickhoff CR, Eickhoff SB, Coull JT, Tahmasian M (2023) Embodying time in the brain: a multi-dimensional neuroimaging meta-analysis of 95 duration processing studies. Neuropsychol Rev.
Narain D, Remington ED, Zeeuw CI, Jazayeri M (2018) A cerebellar mechanism for learning prior distributions of time intervals. Nat Commun 9:469.
Peterburs J, Desmond JE (2016) The role of the human cerebellum in performance monitoring. Curr Opin Neurobiol 40:38–44.
Petzschner FH, Glasauer S, Stephan KE (2015) A Bayesian perspective on magnitude estimation. Trends Cogn Sci 19:285–293.
Pouthas V, George N, Poline JB, Pfeuty M, Vandemoorteele PF, Hugueville L, Ferrandez AM, Lehéricy S, Lebihan D (2005) Neural network involved in time perception: an fMRI study comparing long and short interval estimation. Hum Brain Mapp 25:433–474.
Protopapa F, Hayashi MJ, Kulashekhar S, van der ZW, Battistella G, Murray MM, Kanai R, Bueti D (2019) Chronotopic maps in human supplementary motor area. PLoS Biol 17:e3000026.
Rattat AC, Droit-Volet S (2012) What is the best and easiest method of preventing counting in different temporal tasks? Behav Res Methods 44:67–80.
Repp BH, Su YH (2013) Sensorimotor synchronization: a review of recent research (2006–2012). Psychon Bull Rev 20:403–452.
Riemer M, Kubik V, Wolbers T (2019) The effect of feedback on temporal error monitoring and timing behavior. Behav Brain Res 369:111929.
Rousselet GA, Wilcox RR (2018) Reaction times and other skewed distributions: problems with the mean and the median. BioRxiv 383935.
Salvioni P, Murray MM, Kalmbach L, Bueti D (2013) How the visual brain encodes and keeps track of time. J Neurosci 33:12423–12429.
Sarafyazd M, Jazayeri M (2019) Hierarchical reasoning by neural circuits in the frontal cortex. Science 364:1–9.
Schlerf J, Ivry RB, Diedrichsen J (2012) Encoding of sensory prediction errors in the human cerebellum. J Neurosci 32:4913–4922.
Shea N, Boldt A, Bang D, Yeung N, Heyes C, Frith CD (2014) Supra-personal cognitive control and metacognition. Trends Cogn Sci 18:186–193.
Shuler MG, Bear MF (2006) Reward timing in the primary visual cortex. Science 311:1606–1609.
Simen P, Balci F, deSouza L, Cohen J, Holmes P (2011) A model of interval timing by neural integration. J Neurosci 31:9238–9253.
Skye J, Bruss J, Herbet G, Tranel D, Boes AD (2022) Lesion localization of time disorientation in patients with focal brain damage. BioRixV, https://www.biorxiv.org/content/10.1101/2022.05.24.493338v2
Sohn H, Narain D, Meirhaeghe N, Jazayeri M (2019) Bayesian computation through cortical latent dynamics. Neuron 103:934–947.e5.
Tanaka H, Ishikawa T, Lee J, Kakei S (2020) The cerebro-cerebellum as a locus of forward model: a review. Front Syst Neurosci 14:1–16.
Ullsperger M, Fischer AG, Nigbur R, Endrass T (2014) Neural mechanisms and temporal dynamics of performance monitoring. Trends Cogn Sci 18:259–267.
Üstün S, Kale EH, Çiçek M (2017) Neural networks for time perception and working memory. Front Hum Neurosci 11:83.
Utevsky AV, Smith DV, Huettel SA (2014) Precuneus is a functional core of the default-mode network. J Neurosci 34:932–940.
Wang J, Narain D, Hosseini EA, Jazayeri M (2018) Flexible timing by temporal scaling of cortical responses. Nat Neurosci 21:102–110.
Wiener M, Michaelis K, Thompson JC (2016) Functional correlates of likelihood and prior representations in a virtual distance task. Hum Brain Mapp 37:3172–3187.
Yallak E, Balcı F (2022) Metric error monitoring for a cleaner record of timing. J Exp Psychol Hum Percept Perform 48:1130–1136.
Yeşilyurt B, Uğurbil K, Uludağ K (2008) Dynamics and nonlinearities of the BOLD response at very short stimulus durations. Magn Reson Imaging 26:853–862.